

1 **Hydraulic Redistribution Decreases with Precipitation Magnitude and Frequency in a**  
2 **Dryland Ecosystem: A Data-Model Fusion Approach**

3 Aneesh Kumar Chandel<sup>1</sup>, Mitra Cattray<sup>3</sup>, Yu Zhou<sup>4</sup>, Hang Duong<sup>2,5</sup>, Marcy Litvak<sup>2</sup>, William  
4 Pockman<sup>2</sup> and Yiqi Luo<sup>1</sup>

5 <sup>1</sup>School of Integrative Plant Science, Cornell University, Ithaca, NY, USA

6 <sup>2</sup>Biology Department, University of New Mexico, Albuquerque, NM, USA

7 <sup>3</sup>Department of Earth and Environmental Engineering, Columbia University, USA

8 <sup>4</sup>Department of Environmental Systems Science, ETH Zurich, Switzerland

9 <sup>5</sup>Vietnam National University of Agriculture, Hanoi, Vietnam

10 Corresponding Authors: Aneesh Kumar Chandel ([akc76@cornell.edu](mailto:akc76@cornell.edu)), Yiqi Luo

11 ([y12735@cornell.edu](mailto:y12735@cornell.edu))

12

13

14

15

16

17

18

19

20

21 **Abstract**

22 Hydraulic redistribution (HR), the movement of water via plant root systems that connect soil  
23 compartments with different water potential, should influence soil moisture dynamics  
24 particularly in dryland ecosystems, where water availability strongly constrains ecosystem  
25 function. Realistic representation of HR in ecosystem models is essential to improve the ability  
26 of these models to predict ecosystem function in dryland regions. In this study, we integrated HR  
27 into the Terrestrial ECOsystem model and employed a Bayesian Markov Chain Monte Carlo  
28 technique to optimize soil hydraulic parameters and root conductance using four years of soil  
29 moisture observations from a piñon-juniper woodland. We found that (i) integrating HR  
30 generally improved model prediction of soil moisture during dry periods, particularly in the top  
31 30 cm of the soil profile, where more than 50% of root biomass exists; (ii) HR increased surface  
32 soil moisture by up to 60% during dry periods; (iii) HR decreased with increasing precipitation  
33 magnitude and frequency, however, the length of dry spells between rainfall events also  
34 influenced HR rates; and (iv) upward HR in the top 60 cm soil profile became more pronounced  
35 as dry conditions progressed, with rates ranging from 0.10 to 0.50 mm d<sup>-1</sup>. These findings  
36 highlight that HR plays a critical role in sustaining soil moisture during extended dry periods and  
37 has a limited effect during precipitation events. Future research should investigate the effect of  
38 HR on other ecosystem processes, such as net ecosystem exchange of carbon and  
39 evapotranspiration under varying climatic conditions.

40

41

42

## 43 **1. Introduction**

44 Soil volumetric water content (VWC), defined as the amount of water stored in the  
45 unsaturated zone of the soil profile, is a fundamental state variable regulating ecosystem water  
46 and energy exchanges, particularly in dryland ecosystems (Seneviratne et al., 2010). Drylands  
47 cover over 40% of Earth's terrestrial surface and support more than 38% of the global population  
48 (Prävālie, 2016), underscoring the importance of understanding soil moisture dynamics in these  
49 regions. While VWC provides a useful measure of soil water status, the movement and  
50 availability of this water are governed by soil water potential, particularly its matric component,  
51 which reflects the capillary and adsorptive forces binding water to soil particles (Hillel, 2003;  
52 Novick et al., 2022). In unsaturated soils, matric potential determines how tightly water is  
53 retained and how readily it can move toward plant roots. Because dryland ecosystem functioning  
54 is strongly constrained by precipitation variability (Beer et al., 2010; Ukkola et al., 2021),  
55 understanding how plants regulate water under fluctuating moisture conditions is essential for  
56 predicting ecosystem stability.

57 One key mechanism underlying this regulation is hydraulic redistribution (HR), the passive  
58 movement of water through plant roots, usually at night, from wet to dry regions of the plant  
59 rooting volume driven by differences in water potential. This passive process can favor plant  
60 survival during droughts by tapping into deep soil layers having relatively higher water potential  
61 and redistributing water to the shallow root zone (upward HR) (Nadezhdina et al., 2015; Prieto et  
62 al., 2012; Nicola and Ram, 2022). During wet seasons, HR can redistribute water from wet  
63 surface soil into deeper, drier soil (downward HR), supplementing the infiltration process in  
64 recharging deeper soil layers (Hultine et al., 2003; Scott et al., 2008; Fu et al., 2016; Bleby et al.,  
65 2010). Despite its potential role in regulating plant and ecosystem productivity, nutrient cycling

66 and soil microbial activity (Grünzweig et al., 2022; Sardans and Peñuelas, 2014), most current  
67 dynamic global vegetation models and Earth system model still lack an explicit representation of  
68 HR (Fu et al., 2016).

69 HR has been observed across diverse ecosystems and plant species (Neumann and Cardon,  
70 2012; Nadezhdina et al., 2010; Yu et al., 2013; Priyadarshini et al., 2016). It is recognized as a  
71 structural driver of dryland plant communities, regulating ecosystem productivity, and enhancing  
72 resilience to climate extremes (Lee et al., 2018; Barron - Gafford et al., 2021; Barron - Gafford  
73 et al., 2017; Hafner et al., 2020). The dynamics of HR are influenced by various biotic (rooting  
74 architecture, plant capacitance, transpiration demand, senescence, and dormancy), abiotic factors  
75 (soil hydraulic characteristics, soil moisture status), and climatic conditions (precipitation)  
76 (Prieto et al., 2012; Katul and Siqueira, 2010; Wei et al., 2022). While several studies in arid and  
77 semi-arid ecosystems have reported upward HR during dry periods (Hao et al., 2013a; Lee et al.,  
78 2018; Scott et al., 2008; Yu et al., 2013) and downward HR following precipitation (Hultine et  
79 al., 2003), study on the fine-scale temporal variability of HR across multiple soil depths and  
80 multi-year timescales remains limited. Moreover, a quantitative understanding of how  
81 precipitation magnitude and frequency, key limiting factors in dryland ecosystems, influence HR  
82 rates is still lacking.

83 In this study, we explicitly test two hypotheses: (1) Direction of HR: Upward HR should be  
84 the dominant form of HR in dryland ecosystem. This is due to the recharge of deeper soil layers  
85 from precipitation which can retain moisture for longer periods, and during dry periods roots  
86 facilitate the movement of this retained water to the drier surface soils. (2) HR-precipitation  
87 relationship: Upward HR should decline following precipitation events, reaching its maximum  
88 rates during prolonged dry periods as drought creates steep water potential gradients between

89 deeper, moist soil layers and the drier surface layers, facilitating the upward redistribution of  
90 water.

91 Meanwhile, soil moisture dynamics are governed by a complex interplay of forces that drive  
92 water movement through the soil profile. The primary drivers include matric potential (capillary  
93 and adsorptive forces binding water to soil particles), gravitational potential (driving downward  
94 drainage), and HR (Caldwell et al., 1998). These forces collectively determine soil water  
95 retention, redistribution, and plant water availability (Hillel, 2003). However, isolating their  
96 individual contributions from field soil moisture observations is challenging, because these  
97 processes operate simultaneously and are strongly influenced by soil properties, root activity, and  
98 atmospheric conditions. Consequently, a data-model fusion approach, which integrates process-  
99 based models with soil moisture observations, provides a robust framework to isolate and  
100 quantify HR, offering a more mechanistic and quantitative understanding of soil-plant water  
101 dynamics.

102 Several modeling studies have incorporated various HR schemes into process-based models  
103 to improve understanding of hydrological and ecological processes (Ryel et al., 2002; Amenu  
104 and Kumar, 2008; Wu et al., 2020; Fu et al., 2016; Zheng and Wang, 2007; Tang et al., 2015;  
105 Lee et al., 2018; Quijano and Kumar, 2015). However, realistic representation and estimation of  
106 parameters related to HR remains a challenge, as neither the magnitude of HR nor its associated  
107 parameters can be directly observed in the soil (Ryel et al., 2002; Quijano and Kumar, 2015). As  
108 a result, most models rely on default HR parameter values derived from Ryel et al. (2002). For  
109 example, in a study by Fabian et al. (2010), the maximum soil-root radial conductance ( $C_{RT}$ ), a  
110 key parameter controlling HR, was assigned as the mean value between  $C_{RT}$  reported by Ryel et  
111 al. (2002) for *Artemisia tridentata* and by Williams et al. (1996) for *Quercus-Acer* stand.

112 Similarly, Zheng and Wang (2007) and Yan and Dickinson (2014) prescribed a constant  $C_{RT}$   
113 value based on Ryel et al. (2002). Alternatively, some studies estimated parameters during  
114 specific periods of time when upward or downward HR is assumed negligible, such as wet or dry  
115 season (Fu et al., 2018; Fu et al., 2016). These challenges in direct measurement, the reliance on  
116 assumed parameter values, and the parameterization of HR under the assumption of negligible  
117 redistribution constitute key gaps in our understanding of HR dynamics.

118 To address these gaps, we focused on piñon-juniper (PJ) woodlands, the most widespread  
119 semi-arid ecosystem in the US. PJ woodlands are spatially widespread, ecologically important,  
120 temporally dynamic, and structurally unique dryland ecosystem in the western US, spanning 10  
121 US states and 40 million hectares across the American Southwest (Eastburn et al., 2024; Romme  
122 et al., 2009). Despite their importance, HR has not been previously studied in PJ woodlands.  
123 However, our continuous root sap flux measurements provided direct evidence of HR in both  
124 piñon and juniper roots, indicated by sustained negative root sap flux during nighttime at the  
125 study site (Fig. S1).

126 In this study, we used the process-based Terrestrial ECOsystem (TECO) model to (i) develop  
127 and implement a data assimilation approach to integrate HR into the TECO model; (ii) quantify  
128 and characterize the magnitude and dynamics of HR across multiple soil depths; and (iii) analyze  
129 the temporal patterns of HR and its relationship with precipitation magnitude and frequency. The  
130 TECO model is a well-established ecosystem model that integrates ecological processes to  
131 simulate carbon, water, and energy fluxes within terrestrial ecosystems (Weng and Luo, 2008).  
132 We employed data assimilation to constrain the TECO model including HR using four years of  
133 soil moisture data measured at multiple soil depths, encompassing both wet and dry periods.

## 134 2. Data and Methods

### 135 2.1 Study site and data

136 Our modeling study utilized data from a PJ woodland plot (Lat. 35.642, Long. -104.607,  
137 elevation 1925 m) located in New Mexico, USA, and previously described in Schwinning et al.  
138 (2020). The site is a private ranch covering an area of over 6800 hectares that was ungrazed  
139 from 2012 through the measurement period used for this study and is characterized by a semi-  
140 arid climate. Mean annual precipitation of the site is approximately 460 mm, with the majority  
141 falling between May and October, and a mean annual temperature of 10.5 °C. The soil texture at  
142 the site varies with depth, ranging from loam to clay loam. The vegetation consists of distinct  
143 tree clusters dominated by piñon pine (*Pinus edulis* (Englem.)) and juniper (*Juniperus*  
144 *monosperma* (Englem.) Sarg.) separated by open areas of bare soil and herbaceous cover.

145 VWC was continuously monitored using multi-sensor frequency domain capacitance probes  
146 (Decagon EC-5) installed at four depths (5, 15, 30 and 60 cm), in four soil pits under the tree  
147 canopies. All sensors were monitored every minute by a datalogger (model CR6, Campbell  
148 Scientific), and 15-minute averages were stored. For model parameterization, we used 15-min  
149 VWC records aggregated to daily means. Each sensor was calibrated in the lab before  
150 installation for both air and water frequency. Because soil temperature can affect both soil  
151 permittivity and the response of capacitance sensors, potentially confounding the small  
152 fluctuations in VWC caused by HR, temperature correction factors were applied to the measured  
153 VWC at each depth, using the nearest measured temperature, following the method described by  
154 Saito et al. (2009). Rather than excluding data below 0 °C, we used this temperature-correction  
155 approach to reduce the influence of temperature-driven artifacts on the soil moisture signal. This

156 strategy allows retention of continuous soil moisture records while accounting for the known  
157 sensitivity of capacitance sensors to temperature-dependent changes in dielectric permittivity.

## 158 **2.2 Modeling framework**

159 TECO is a process-based ecosystem model (Hou et al., 2021; Jiang et al., 2018; Weng and  
160 Luo, 2008), and has evolved from the TCS model (Luo and Reynolds, 1999). The model consists  
161 of major components: canopy photosynthesis, plant growth, soil water dynamics, and soil carbon  
162 transfers. The canopy photosynthesis and soil water dynamics submodels run at the hourly time  
163 step whereas the plant growth and soil carbon submodels run at the daily time step. The model is  
164 driven by seven environmental variables, including precipitation (mm), wind speed ( $\text{m s}^{-1}$ ), solar  
165 radiation ( $\text{W m}^{-2}$ ), air and soil temperature (C), relative humidity (%), and vapor pressure deficit  
166 (kPa). The detailed description of TECO model is available (Weng and Luo, 2008) and only a  
167 brief description of soil water dynamics is provided here.

168 The soil profile is divided into 10 layers with a total depth of 180 cm, with varying thickness:  
169 5 cm for the first layer, 10, 15, and 30 cm for the second, third, and fourth layers respectively,  
170 and 20 cm for each of the fifth through tenth layers. VWC in each layer results from the mass  
171 balance between influx and efflux, with changes primarily attributed to vertical unsaturated flow,  
172 transpiration, precipitation, runoff, and drainage. Evaporation depletes water from the first two  
173 soil layers, while transpiration depletes water from all soil layers containing roots, allocated  
174 based on root fraction in each layer (Eq. 8). Given the predominantly arid conditions of the study  
175 site, runoff and drainage were found negligible. Thus, water movement between soil layers is  
176 simulated as follows:

$$177 \quad \frac{dW_i}{dt} = \frac{dF_i}{dz} - E_i - T_i \quad (1)$$

178 where  $W_i$  is the water storage (cm) in layer  $i$ ,  $t$  is time (h),  $F_i$  is net unsaturated flow of water into  
 179 layer  $i$  (cm h<sup>-1</sup>),  $z$  is vertical thickness,  $E_i$  and  $T_i$  are evaporation and transpiration water loss from  
 180 layer  $i$  (cm h<sup>-1</sup>).

181 The unsaturated soil water movement is simulated vertically according to modified form of  
 182 Buckingham-Darcy's law (Campbell, 1985) (Eq. 2), with Brooks (1965) equation (Eq. 4)  
 183 estimating hydraulic conductivity and soil water retention curve (SWRC) to simulate soil water  
 184 potential ( $\Psi$ ).

$$185 \quad \frac{dF_i}{dz} = K(\theta_i) \left( \frac{d\Psi_i}{dz} + 1 \right) \quad (2)$$

186 where  $K(\theta_i)$  is the unsaturated soil hydraulic conductivity (cm h<sup>-1</sup>) for VWC  $\theta$  (cm<sup>3</sup> cm<sup>-3</sup>) in  
 187 layer  $i$ ,  $\Psi_i$  is soil water matric potential (MPa) in layer  $i$ , and  $z$  is the vertical thickness (cm) of  
 188 the soil.

$$189 \quad K(\theta_i) = K_s \left[ \frac{\theta_i - \theta_r}{\theta_s - \theta_r} \right]^{(2m+3)} \quad (3)$$

190 where,  $K_s$  is the soil saturated hydraulic conductivity (cm h<sup>-1</sup>),  $m$  is the pore size distribution  
 191 index,  $\theta_s$  and  $\theta_r$  are saturated and residual VWC (cm<sup>3</sup> cm<sup>-3</sup>)

$$192 \quad \frac{\theta - \theta_r}{\theta_s - \theta_r} = \left( \frac{\Psi}{\Psi_b} \right)^{-1/m} \quad (4)$$

193  $\Psi_b$  is the soil air entry water potential.

194 To quantify the direction and magnitude of HR, we integrated the HR model by Ryel et al.  
 195 (2002) into equation 1 of TECO model (Eq. 5). This HR model empirically describes HR flux  
 196 based on the soil water potential gradient between two soil layers (Eq. 6). HR was assumed to  
 197 occur only at night, with its occurrence controlled by solar radiation instead of fixed day and  
 198 night hours. Daytime starts as solar radiation exceeds 10 W m<sup>-2</sup>, thereby inhibiting HR since the  
 199 water potential gradient typically favors water movement from roots to canopy to meet

200 transpiration demand during the day. This pattern is evident in Fig. S1, where under low or zero  
 201 solar radiation, root sap flux was found to be negative, indicating water movement away from  
 202 the root zone which is an indicator of occurrence of HR at the study site. Using these  
 203 assumptions, the net water movement into soil layer  $i$  from other soil layers  $j$  can be expressed  
 204 as:

$$205 \quad \frac{dW_i}{dt} = \frac{dF_i}{dz} - E_i - T_i + H_i \quad (5)$$

$$206 \quad H_i = C_{RT} \sum (\Psi_j - \Psi_i) \max(c_i, c_j) \frac{R_i R_j}{1 - R_x} D_{tran} \quad (6)$$

$$207 \quad c_i = \frac{1}{1 + \left(\frac{\Psi_i}{\Psi_{50}}\right)^b} \quad (7)$$

$$208 \quad R_i = \frac{R_0}{1 + \left(\frac{d}{d_{50}}\right)^a} \quad (8)$$

209 where in Eq 6,  $H_i$  is the net water redistributed by roots into layer  $i$  ( $\text{cm h}^{-1}$ ) from other soil  
 210 layers  $j$ ,  $C_{RT}$  is the maximum radial soil-root conductance of the entire active root system for  
 211 water ( $\text{cm MPa}^{-1} \text{h}^{-1}$ ),  $\Psi$  is soil matric potential (MPa),  $c_i$  is a factor reducing soil-root  
 212 conductance based on  $\Psi_i$ ,  $R_i$  is the fraction of active roots in layer  $i$ ,  $R_0$  is the average vertically  
 213 summed root dry mass from the bottom to the root zone to the soil surface, and  $D_{tran}$  is a factor  
 214 reducing water movement among layers by roots while plant is transpiring and is assumed to be  
 215 1 during the night when transpiration is minimal and 0 during day.  $R_x = R_i$  when  $\theta_i > \theta_j$  or  $R_x = R_j$   
 216 when  $\theta_j > \theta_i$ . In Eq 7,  $\Psi_{50}$  is the soil water potential (MPa) where conductance is reduced by  
 217 50% and  $b$  is an empirical constant. In Eq 8,  $d$  is soil depth (cm), and  $d_{50}$  is the soil depth at the  
 218 median of the root distribution and  $a$  is a shape parameter (Table 1). The Brooks (1965) model  
 219 for SWRC was utilized to simulate soil water potential ( $\Psi$ ), facilitating the development of soil  
 220 water potential gradients necessary for HR by tree roots (Eq. 4). Due to lack of site-specific

221 parameters, the default values of  $b$  and  $\Psi_{50}$  were used as 3.22 and -1 MPa, respectively (Ryel et  
222 al., 2002).

### 223 **2.3 Data assimilation for parameters estimation**

224 We used Bayesian probabilistic inversion to calibrate parameters associated with soil  
225 hydraulics, where posterior probability density functions of parameters are obtained from prior  
226 knowledge about the parameters and the error between model and observations. According to  
227 Mosegaard and Sambridge (2002), Bayesian inversion can be summarized by the following  
228 equation:

$$229 \quad p(c|Z) \propto p(Z|c) p(c) \quad (9)$$

230 where  $p(c|Z)$  is posterior probability density function of model parameters  $c$ ;  $p(Z|c)$  is a  
231 likelihood function of parameters  $c$ ;  $p(c)$  is prior probability density function of parameters  $c$ . We  
232 assumed that the prediction errors were normally distributed and uncorrelated, hence, the  
233 likelihood function,  $p(Z|c)$ , was calculated as follows:

$$234 \quad p(Z|c) \propto \exp\left\{-\sum_{i=1}^k \frac{(Z_i - X_i)^2}{2\sigma_i^2}\right\} \quad (10)$$

235 where  $Z_i$  is observed VWC at  $i^{\text{th}}$  soil layer,  $X_i$  is VWC simulated by TECO at a corresponding  
236 soil depth;  $\sigma_i^2$  is the variance of a measurement at a soil layer;  $k$  is the total number of soil layers.

237 To generate the posterior distributions, we first specified the priors of the parameters to be  
238 uniformly distributed over the intervals specified in Table 1. We put constraints on parameters  
239 based on literature. The initial set of parameters was randomly selected within the prior  
240 parameter ranges. Once we specified parameter ranges, we used the Metropolis-Hastings (M-H)  
241 algorithm (Hastings, 1970; Metropolis et al., 1953), a Markov chain Monte Carlo method, to

242 sample from the posterior parameter distribution. To generate a parameter set, we ran M-H  
 243 algorithm in two steps: proposing step and moving step. In the proposing step, a new parameter  
 244 set  $c^{new}$  was generated from a previously accepted parameter set  $c^{k-1}$  through a proposal  
 245 distribution ( $c^{new}|c^{k-1}$ ):

$$246 \quad c^{new} = c^{k-1} + r \times \frac{c^{max} - c^{min}}{D} \quad (11)$$

247 The value of  $P(c^{k-1}|c^{new})$  was then compared with a random number  $U$  from 0 to 1. Parameter set  
 248  $c^{new}$  was accepted if  $P(c^{k-1}|c^{new}) \geq U$ , otherwise  $c^k$  was set to  $c^{k-1}$ . In the moving step, a  
 249 probability of acceptance  $P(c^{k-1}|c^{new})$  was calculated as in the following (Marshall et al., 2004):

$$250 \quad P(c^{k-1}|c^{new}) = \min \left\{ 1, \frac{p(Z|c^{new})p(c^{new})}{p(Z|c^{k-1})p(c^{k-1})} \right\} \quad (12)$$

251 The M-H algorithm was repeated for 50,000 simulations, and then all accepted parameters  
 252 values were used to generate the probability distribution functions (Xu et al., 2006).

253 To evaluate the impact of HR on soil moisture dynamics in a PJ woodland, we conducted  
 254 two multi-year simulations using two configurations of the TECO model: TECO+HR (with HR)  
 255 and default TECO (HR turned off). To distinguish the influence of HR from soil hydraulic  
 256 properties, we adopted a data assimilation approach focused on calibrating only the TECO+HR  
 257 model. Soil moisture observations were available at 5, 15, 30 and 60 cm depths, and data  
 258 assimilation was therefore applied only to these four soil layers over a four-year period, and data-  
 259 model comparisons are presented exclusively for these depths. The parameters values deeper  
 260 than 60 cm were not calibrated and were empirically defined from literature values. This  
 261 modeling strategy is consistent with other data assimilation studies, in which model calibration is  
 262 restricted to soil layers with available observations (Fu et al., 2016; Zhang et al., 2016). In total,

263 21 parameters were optimized including 20 soil hydraulic parameters ( $\theta_s$ ,  $\theta_r$ ,  $K_s$ ,  $m$ , and  $\Psi_b$  for  
264 each of the four soil depths) across four soil layers and one HR-related parameter ( $C_{RT}$ ). The  
265 prior range of soil hydraulic parameters were informed by established relationships between soil  
266 texture and hydraulic properties (Rawls et al., 1982; Clapp and Hornberger, 1978). The prior  
267 range for  $C_{RT}$  was based on values reported in Fu et al. (2016). Within this range, we optimized  
268 depth-specific soil hydraulic parameters to achieve a close match between modeled and observed  
269 soil moisture (Table 1).

270 After calibrating the TECO+HR model, we deactivated the HR process and ran simulations  
271 with the same optimized parameters to generate the default TECO scenario. Before each model  
272 simulation, we performed a 200-year spin-up separately for both model configuration  
273 (TECO+HR with HR active and default TECO with HR disabled) to ensure that each model  
274 reached stable carbon stocks as initial conditions.

275 The motivation to calibrate only TECO+HR model, rather than the default TECO is to avoid  
276 parameter compensation for unresolved processes (Luo and Schuur, 2020), in which the absence  
277 of HR could lead to unrealistic adjustments of soil hydraulic parameters to indirectly capture its  
278 effects. This approach allowed us to ensure that differences in soil moisture dynamics between  
279 TECO+HR and default TECO simulations were attributable solely to the presence or absence of  
280 HR.

281 Furthermore, to evaluate the influence of cumulative precipitation and soil moisture memory  
282 on HR, we calculated the Antecedent Precipitation Index (API) for the study period (2018–2021)  
283 following Kohler and Linsley (1951). API acts as a proxy for soil moisture status by accounting

284 for the decaying effect of past rainfall events. The daily API ( $API_t$ ) was calculated using the  
285 recursive decay function:

$$286 \quad \quad \quad API_t = P_t + (k * API_{t-1}) \quad \quad \quad (13)$$

287 where  $P_t$  is the precipitation on day  $t$  (mm),  $API_{t-1}$  is the index value of the preceding day,  
288 and  $k$  is a decay constant representing the recession of soil moisture due to evapotranspiration  
289 and drainage. We used a decay constant of  $k = 0.90$ , which falls within the commonly applied  
290 range for antecedent precipitation indices and is consistent with optimization analyses indicating  
291 optimal decay constants near 0.90 (Li et al., 2021). This metric enables differentiation between  
292 short dry intervals following wet conditions and extended dry spells with limited antecedent  
293 moisture.

#### 294 **2.4 Statistical analysis**

295 Model performance was assessed by comparing simulated outputs with observed data during  
296 full simulation periods (2018- 2021), dry, and wet periods, defined as days without and with  
297 rainfall events, respectively. During the study period, wet days accounted for 22% of all days,  
298 whereas dry days comprised the remaining 78%. Model performance was evaluated using two  
299 statistical metrics: root mean square error (RMSE) and absolute mean error (MAE). RMSE is  
300 widely used to quantify model accuracy, but its squared-error formulation overemphasizes the  
301 effects of large deviations (Willmott and Matsuura, 2005). Therefore, MAE was also calculated  
302 as a measure of the average magnitude of deviation from observed values (Alfieri et al., 2017).  
303 Both metrics were calculated as follows:

$$304 \quad \quad \quad RMSE = \sqrt{\frac{1}{n} \sum_{i=1}^n (m_i - o_i)^2} \quad \quad \quad (14)$$

305 
$$MAE = \frac{1}{n} \sum_{i=1}^n |m_i - o_i|^2 \quad (15)$$

306 Where:  $o_i$  represents observed values,  $m_i$  represents modeled values, and  $n$  represents the  
307 number of data points.

Table 1: Parameters constrained using data assimilation in the TECO model from soil moisture data from 2018 to 2021.

Parameters	Symbols	Constrained values	Range	Units	References
Saturated water content	$\theta_s$	0.34/0.38/0.36/0.33	[0.3, 0.4]	$\text{cm}^3 \text{cm}^{-3}$	Calibrated
Residual water content	$\theta_r$	0.05/0.07/0.06/0.03	[0, 0.08]	$\text{cm}^3 \text{cm}^{-3}$	Calibrated
Saturated hydraulic conductivity	$K_s$	0.14/0.29/0.30/0.70	[0.1, 2]	$\text{cm h}^{-1}$	Calibrated
Pore size distribution	$m$	0.89/0.66/0.88/0.84	[0, 1]	-	Calibrated
Air entry water potential	$\Psi_b$	96/60/50/40	[0, 100]	cm	Calibrated
Maximum radial soil-root conductance	$C_{RT}$	0.022	[0, 1]	$\text{cm MPa}^{-1} \text{h}^{-1}$	Calibrated
Soil $\Psi$ where root conductivity reduced by 50%	$\Psi_{50}$	-1.0	-	MPa	(Ryel et al., 2002)
Empirical constant	$b$	3.22	-	-	(Ryel et al., 2002)
Average vertically summed root dry mass	$R_0$	0.90	-	$\text{kg m}^{-2}$	(Schwinning et al., 2020)
Soil depth at the median of the root distribution	$D_{50}$	25	-	cm	(Schwinning et al., 2020)
Root distribution shape parameter	$a$	2.2	-	-	(Schwinning et al., 2020)

Four values represent parameters in the four modeled VWC at depths of 5, 15, 30, and 60 cm, respectively.

310 **3. Results**

311 **3.1 Parameter estimation via data assimilation and water mass balance**

312 The data assimilation approach, using VWC data to constrain the model, yielded well-  
313 constrained soil hydraulic parameters (Table 1; Fig. S2 and S3). The resulting posterior  
314 probability density functions, characterized by sharp peaks, narrow spread, and consistency  
315 across soil depth support the reliability and accuracy of these calibrated parameter values.  
316 Additionally, soil water mass balance of soil profile was conserved before and after  
317 incorporating the HR process into the TECO model (Fig. S4). The key components of the water  
318 budget: precipitation, evapotranspiration, and changes in soil water content remained balanced,  
319 ensuring that the model accounted for all water fluxes. Furthermore, the sum of HR across all  
320 soil layers (10 layers) was consistently equal to zero, further ensuring that no water was  
321 artificially introduced or lost from the system.

322

323

324

325

326

327

328

329

330

331 **3.2 Observed and simulated soil moisture**

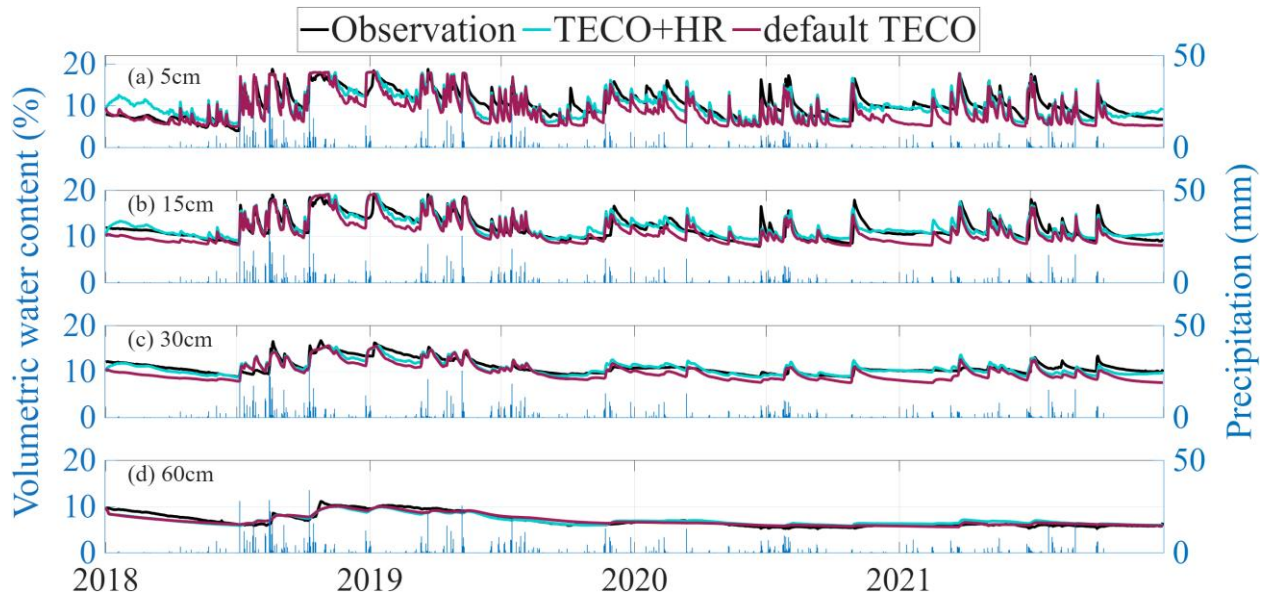


Figure 1a-d: Observed and simulated soil volumetric water content for the year 2019 (January 1, 2018 to December 31, 2021) at soil depths of 5 cm (a), 15 cm (b), 30 cm (c), and 60 cm (d). Black lines indicate observations, cyan lines indicate TECO+HR, and magenta lines indicate default TECO. Vertical blue bars indicate daily precipitation (right axis).

332  
333  
334  
335  
336  
337  
338  
339  
340  
341  
342  
343  
344  
345

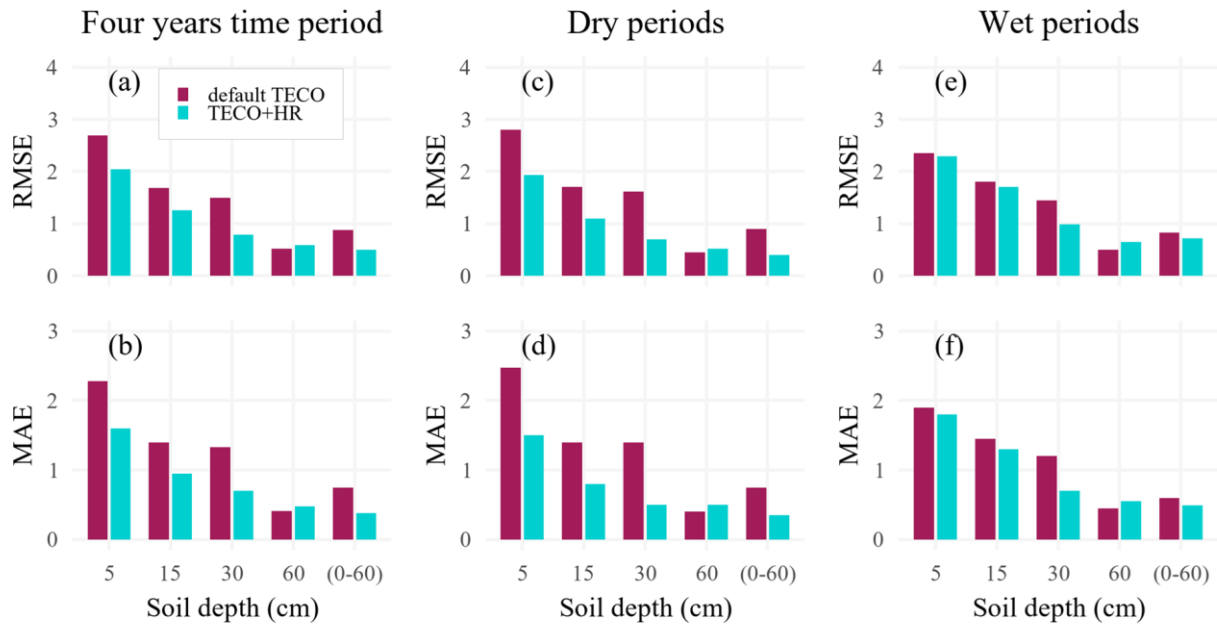


Figure 2: Model performance for soil moisture across different depths (5, 15, 30, and 60 cm, and 0-60 cm integrated soil profile), considering temporal variations in soil moisture conditions. Root Mean Square Error (RMSE) and Mean Absolute Error (MAE) are presented for the complete time series (a, b), dry periods (c, d), and wet periods (e, f). Lower values of RMSE and MAE indicate better model performance.

346

347 The data assimilation-constrained models generally captured both the magnitude and  
 348 dynamics of observational data, reproducing seasonal variations in soil moisture across four soil  
 349 depths. Minor mismatches at the topsoil (5 cm) likely reflect the complexity of near-surface  
 350 processes that are not fully represented in simplified models and potential sensor lag due to  
 351 imperfect soil contact, as similar discrepancies are not observed at deeper layers. In addition,  
 352 following prolonged dry periods, initial rainfall can be largely offset by evaporation, resulting in  
 353 muted surface soil moisture responses (Miele et al., 2023; Cattray et al., 2025; Asadollahi et al.,  
 354 2022). While TECO+HR simulation showed an improvement in the overall model performance,  
 355 the impact of HR was mostly pronounced during dry periods (Figs. 1 and 2). We further  
 356 examined diurnal soil moisture fluctuations (Fig. S5) and found that TECO+HR closely tracked  
 357 the observed diurnal cycles, whereas the default TECO failed to capture this pattern, suggesting

358 that the observed diurnal variability was likely driven by HR. Additionally, we compared min-  
359 max normalized soil matric potential at 15, 30, and 60 cm with simulations derived from Eq. (4)  
360 (Fig. S6). Both models reproduced the general trends of the observations, suggesting that the  
361 simulated soil water potential gradients were consistent with measurement.

362 Moreover, during periods of limited precipitation, the TECO+HR (blue lines) consistently  
363 maintained higher soil moisture compared to default TECO (red lines), aligning closer to  
364 observation particularly in the topsoil layers (Fig. 1a-c). Following precipitation events, the  
365 default TECO and TECO+HR simulations converged, suggesting the minimal influence of HR  
366 under wet conditions at the study site. However, as surface soil moisture decreased following  
367 precipitation, the two simulations diverged again, with TECO+HR maintaining higher moisture  
368 levels in the topsoil layers, highlighting the role of HR in maintaining soil moisture during  
369 prolonged drought.

370 The incorporation of HR into TECO resulted in reductions in model errors. During dry  
371 periods, the RMSE decreased by 25, 43, and 52% at 5, 15, and 30 cm soil depths, respectively.  
372 However, limited improvement was observed at 60 cm soil depth. Correspondingly, the MAE  
373 was reduced by 30, 53, and 60% at 5, 15, and 30 cm, respectively. Over the entire study period,  
374 RMSE decreased by 24, 25, and 47% at 5, 15, and 30 cm, with MAE reductions were 29, 34, and  
375 55% at the same depths (Fig. 2a-d). Overall soil profile performance improved as well, with  
376 RMSE and MAE reductions over 40% for both the four-year simulation and dry periods. These  
377 improvements during dry periods are especially important, as roots are most vulnerable to  
378 drought. By mitigating soil water deficits in surface layers, HR could reduce the risk of hydraulic  
379 failure, thereby supporting plant species survival and it could enable better prediction of  
380 ecosystem responses to water stress, such as carbon uptake (Domec et al., 2010), and

381 evapotranspiration (Zhu et al., 2017). In contrast, during wet periods, HR had minimal influence  
382 on soil moisture (Fig. 2e, f).

### 383 3.3 Effect of HR on soil moisture

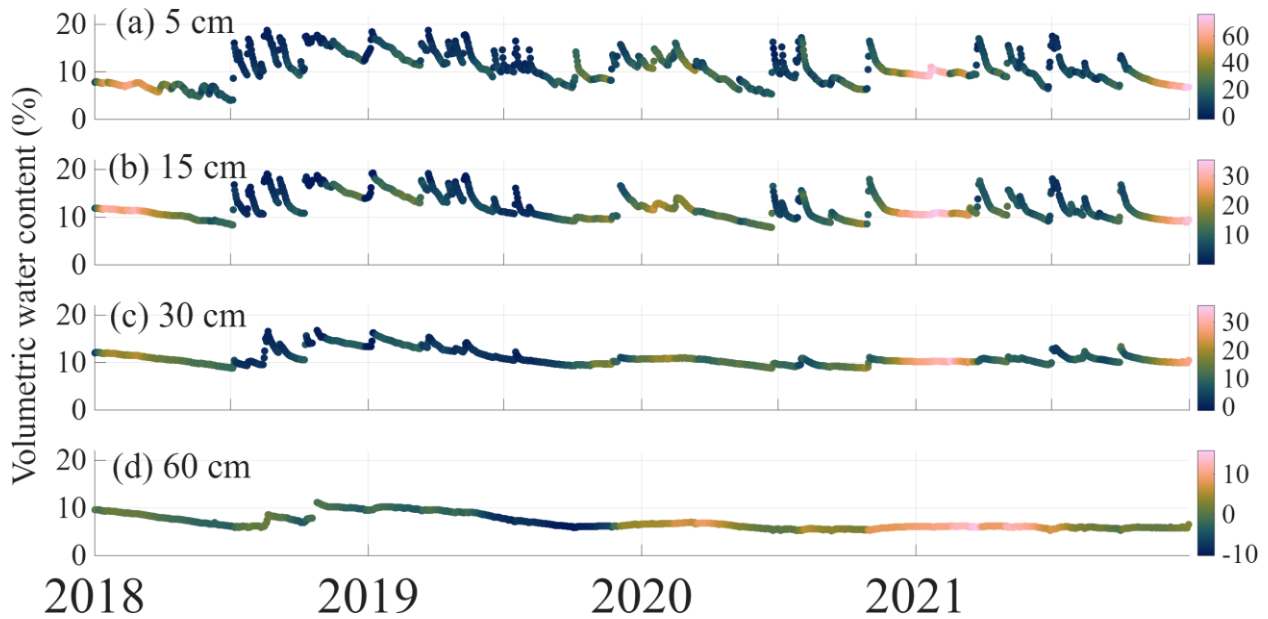


Figure 3: Relative change in modeled volumetric water content (VWC) across four soil depths (5, 15, 30, and 60 cm). The color gradient represents the magnitude of relative change in modeled VWC, calculated as  $(HR - No\ HR) / No\ HR \times 100$ , with HR and No HR indicating simulations with and without hydraulic redistribution, respectively. The relative change is overlaid on observed VWC.

384 The direct impact of HR on hydrological processes should be evident in the soil profile  
385 water content. We tested this by comparing VWC model simulations in TECO with and without  
386 HR processes, to observed VWC time series at four depths (Fig. 3). We found that cumulative  
387 effects of HR on soil moisture vary with depth, primarily due to the non-uniform root biomass  
388 distribution throughout the soil profile (Fig. S8). The most pronounced effects of HR were  
389 observed in the topsoil layers (5, 15, and 30 cm), where average daily water content increased by  
390 up to 60% compared to simulation without HR. This increase was driven by upward HR,  
391 especially during dry-down periods (Fig. 4b).

### 392 3.4 HR simulations

393 Model simulation revealed  
394 distinct patterns of HR dynamics  
395 across soil depths and temporal  
396 scales. Fig. 4 illustrates these patterns  
397 over two timescales: a short-term,  
398 diurnal pattern (Fig. 4a), and a long-  
399 term perspective from 2018 to 2021  
400 (Fig. 4b). HR is a process with both a  
401 source and a sink for water  
402 movement. In Fig. 4, positive HR  
403 suggests that a soil layer is gaining  
404 water (sink), whereas negative HR  
405 values suggest that the layer is losing  
406 water (source).

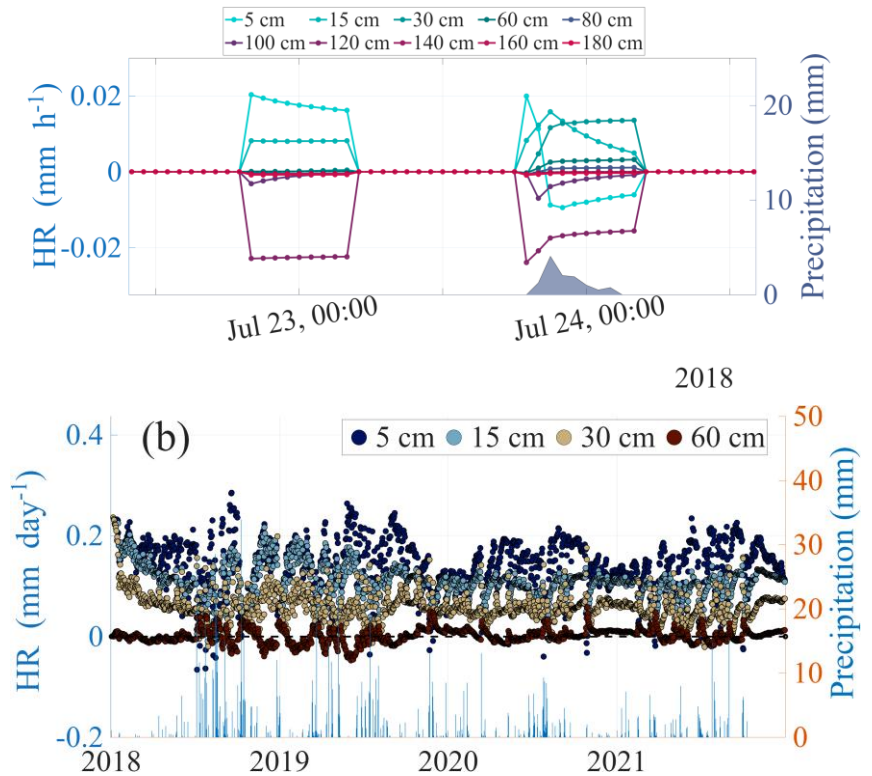


Figure 4: Temporal dynamics of hydraulic redistribution (HR). (a) diurnal pattern of modeled HR across soil depths from July 22-24, 2018. The graph illustrates HR patterns during a dry period followed by a precipitation event (right y-axis). Colored lines represent different soil depths. (b) long-term daily HR trends and precipitation from January 2018 to December 2021. The blue vertical bars represents precipitation (right y-axis).

407 The short-term modeling analysis highlights diurnal pattern of HR during dry conditions and  
408 a precipitation event (Fig. 4a). For instance, on July 23, 2018, during a dry period, upward HR  
409 occurred, moving water from deeper (> 100 cm) to shallower (0-30 cm) soil layers. However,  
410 following a precipitation event on July 24, 2018 (12 mm), this pattern shifted. The top 5 and 15  
411 cm layers showed negative HR and a decrease in the upward HR rate, respectively, acting as a  
412 water source for deeper layers. At the same time, deeper soil layers showed a decline in negative  
413 HR rates, suggesting signs of receiving water likely from the topsoil layers. The sum of HR  
414 across all soil layers remained zero, confirming that HR redistributed water rather than adding to

415 the system. Consequently, downward HR from the topsoil supplemented infiltration, enhancing  
416 water movement into deeper soil layers, reflected by a decrease in the negative HR rates at  
417 depths and an increase in the positive HR rate at 30 cm (Fig. 4a).

418 While our model simulates HR across 10 soil layers, we present long-term results for only  
419 the top four soil layers (5, 15, 30, and 60 cm) to enable direct comparison with the available  
420 observed soil moisture data. A clear seasonal pattern emerged, with HR generally intensifying  
421 during dry periods (Fig. 4b).

422 Our model showed that upward HR was predominantly occurring in up to top 30 cm of soil  
423 profile, with values ranging from -0.066 to 0.29 mm d<sup>-1</sup> in each soil layer and an average of 0.30  
424 mm d<sup>-1</sup> across the top 30 throughout the study period. Downward HR, while less pronounced,  
425 moved water only from the 5 cm soil layer during monsoon seasons and large precipitation  
426 events (e.g., July 2018, 2019, 2020, and 2021; Fig. 4b). In contrast, 60 cm soil layer typically  
427 exhibits a negative HR during dry periods, acting as a water source for upper layers, and positive  
428 HR during wet periods, suggesting occasional water input from surface layers ranging from -  
429 0.096 to 0.059 mm d<sup>-1</sup> (mean 0.0015 mm d<sup>-1</sup>). Moreover, integrated soil profile (top 60 cm of soil  
430 profile), showed that upward HR was the dominant form of HR throughout the year, ranging  
431 from 0.10 to 0.53 mm d<sup>-1</sup> with a mean value 0.31 mm d<sup>-1</sup> (Fig. S7).

432

433

434

435

### 436 3.5 Precipitation influences on HR

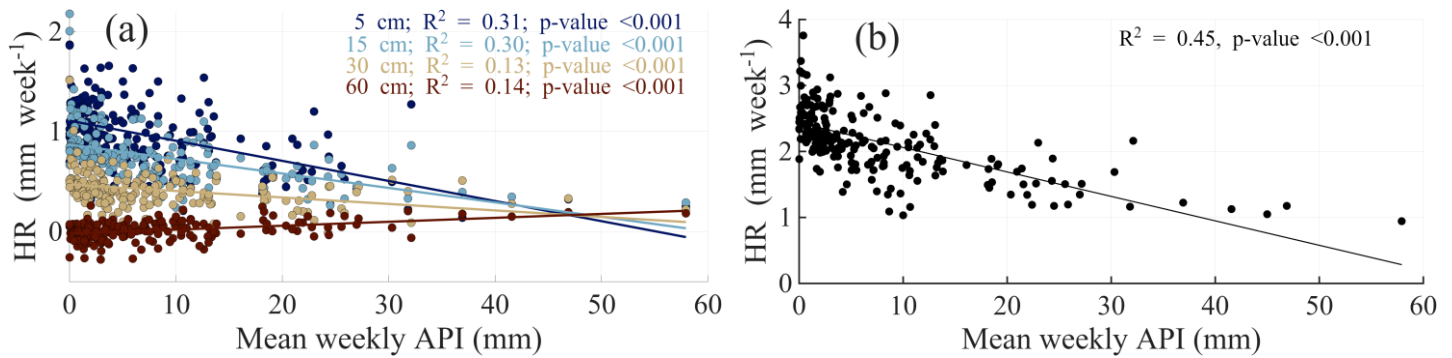


Figure 5: Relationships between hydraulic redistribution (HR) and Antecedent Precipitation Index (API). (a) Weekly HR rates versus mean weekly API at different soil depths (5, 15, 30, and 60 cm). For each soil depth, the trend lines,  $R^2$ , and corresponding p-values are shown. (b) Depth-integrated weekly HR across 0–60 cm soil profile versus mean weekly API, with trend line,  $R^2$ , and p-value.

437 The model results showed a significant linear relationship between weekly HR and mean  
438 weekly API (mm) (Fig. 5a-b). In the topsoil layers (5 cm and 15 cm), HR exhibited negative  
439 relationships with API ( $R^2 = 0.31$  and  $0.30$  respectively, both p-values < 0.001), indicating that  
440 HR activity decreased as antecedent moisture conditions became wetter. In contrast, positive  
441 correlation were observed at 30 and 60 cm depths ( $R^2 = 0.13$  and  $0.14$  respectively, both p-values  
442 < 0.001), suggesting downward redistribution under wetter antecedent conditions.

443 Additionally, when HR was integrated across the soil profile (0-60 cm), a significant  
444 negative relationship with mean weekly API was observed ( $R^2 = 0.45$ , p-values < 0.001, Fig. 5b).  
445 This suggests that overall HR activity was greatest under drier antecedent conditions and  
446 declined as cumulative moisture availability increased, highlighting the stronger role of HR in  
447 regulating soil water dynamics during prolonged dry periods.

448 Despite these clear trends, variability in HR was observed across the full range of mean  
449 weekly API values (Fig. 5a-b). This variability could be attributed to the rainfall frequency,  
450 event size, and the duration of dry periods between rainfall events (Fig. 6), factors that are  
451 implicitly captured by API. Figure 6 provides a more detailed view of these controls by relating

452 HR directly to dry spell length and rainfall  
 453 frequency, suggesting that HR may increase  
 454 not only with reduced precipitation  
 455 frequency but also as the interval between  
 456 consecutive rainfall events lengths. HR. HR  
 457 was lowest under conditions of high rainfall  
 458 frequency and shorter dry spells,  
 459 progressively increasing to its peak in the  
 460 absence of rainfall. However, as the drought  
 461 period extended beyond 30 days, HR  
 462 declined, suggesting potential limitation on

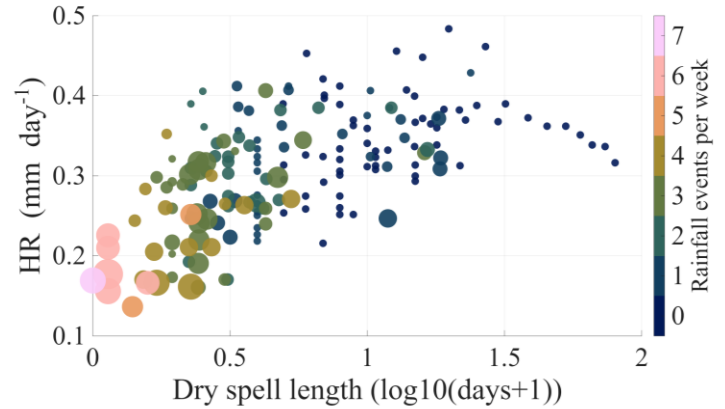


*Figure 6: Relationship between weekly mean hydraulic redistribution ( $\text{mm d}^{-1}$ ), dry spell length between two rainfall events ( $\log_{10}(\text{days}+1)$ ). The color scale indicates the number of rainfall events per week, while marker size represents the weekly precipitation amount ( $\text{mm week}^{-1}$ ). Dry spell length denotes the number of rainless days between two consecutive precipitation events. The x-axis shows dry spell length transformed as  $\log_{10}(\text{days} + 1)$  to allow inclusion of zero-length dry spells.*

463 availability of deeper water to sustain HR. This variability is further illustrated through three  
 464 scenarios (Fig. S7): 1) Following a rainfall event (28 mm on July 5, 2018), HR in the top 60 cm  
 465 of soil profile was minimal at  $0.13 \text{ mm d}^{-1}$ , indicating limited driving force for water  
 466 redistribution when soil moisture was abundant. 2) During a transition period between rainfall  
 467 events (July 5-10, 2018), HR gradually increased but remained moderate, ranging from 0.13 to  
 468  $0.20 \text{ mm d}^{-1}$ , suggesting a progressive activation of the redistribution process as soil began to  
 469 dry. 3) During a prolonged dry period (November 23-30, 2018), HR peaked at  $0.20\text{-}0.52 \text{ mm d}^{-1}$ ,  
 470 demonstrating enhanced redistribution activity in response to the development of soil moisture  
 471 gradients.

472

473

474

## 475 4. Discussion

### 476 4.1 Patterns of hydraulic redistribution

477 Our findings support the hypothesis that upward HR is the dominant form of HR in dryland  
478 ecosystems due to limited precipitation amount and sporadic rainfall events (Fig. S7). This  
479 prevalence of upward water movement is characteristic of semi-arid regions, where deep-rooted  
480 plants often redistribute water from moist deeper layers to drier surface soils during periods of  
481 water stress (Caldwell et al., 1998; Ryel et al., 2002). Notably, the most pronounced HR  
482 occurred in the topsoil layer (5, 15, and 30 cm), (Fig. 4b), which can be attributed to vertical root  
483 distribution, with over 50% of root biomass concentrated in the top 30 cm ( $D_{50} = 25$  cm) of the  
484 soil profile (Fig. S8). Similar relationships between root distribution and HR intensity have been  
485 reported in previous studies, where deeper root systems extend redistribution to deeper soil  
486 layers, whereas shallow root systems amplify HR effects in surface soil due to higher root  
487 density and activity (Hao et al., 2013b).

488 The magnitude of HR simulated in this study (0.10-0.53 mm d<sup>-1</sup> for top 60 cm soil) falls  
489 within the range reported in previous studies. Estimated HR rates for the topsoil were  
490 comparable to values synthesized in the global review by Neumann and Cardon (2012), which  
491 reported HR magnitudes ranging from 0.04 to 3.2 mm d<sup>-1</sup> across ecosystem. However, our  
492 estimates are slightly higher than the upper range reported by Yang et al. (2022) for desert or  
493 sparsely vegetated ecosystems (0.014-0.475 mm d<sup>-1</sup>). These differences likely reflect variations  
494 in vegetation structure, rooting depth, soil texture, and water availability among ecosystems.

495

## 496 **4.2 Effects of precipitation variability on HR**

497 Our findings support the hypothesis that the precipitation pattern significantly influences the  
498 magnitude and variability of HR (Figs. 4a-b, and S7). The rate of HR in the topsoil profile (<60  
499 cm) exhibited a consistent response to precipitation events, characterized by sharp declines  
500 following large rainfall, and a gradual recovery to pre-rain levels during subsequent dry periods.  
501 Similar responses have been reported in previous study, where precipitation temporarily  
502 suppresses HR by reducing water potential gradients between shallow and deeper soil layers  
503 (Hao et al., 2013b). However, as water redistributes through the soil profile, new hydraulic  
504 gradients re-establish, leading to enhanced HR activity. In this phase, roots actively redistribute  
505 water from newly moistened deep layers to drier shallow layers (Yu and D'odorico, 2014; Ryel  
506 et al., 2002).

507 Our model predicted that HR rates were generally higher during rainless periods compared to  
508 rainfall periods within a given year. For instance, during the prolonged dry period in 2020 (driest  
509 year), HR rates remained consistently high, 0.17-0.40 mm d<sup>-1</sup>, with minimal fluctuations. The  
510 consistent high HR rates, likely arises from more pronounced soil water potential gradients  
511 derived from sustained plant water demand and surface evaporation in the absence of frequent  
512 precipitation (Fu et al., 2016; Meinzer et al., 2004).

513 Seasonal patterns include higher HR rates (0.12-0.53 mm d<sup>-1</sup>) during the drier periods  
514 (typically from November to May) and lower rates (0.10-0.30 mm d<sup>-1</sup>) during the monsoon  
515 season (usually from June to October) (Fig. S7). This seasonality underscores the influence of  
516 both precipitation patterns and potential evapotranspiration on HR dynamics, highlighting that  
517 HR is likely more pronounced during drier seasons when soil moisture gradients are likely to be

518 more substantial due to reduced precipitation and potentially higher evaporative demand (Scott et  
519 al., 2008; Fu et al., 2016; Yu and D'odorico, 2014).

#### 520 **4.3 Limitation and future perspectives**

521 While our modeling study provides valuable insights into HR dynamics in PJ woodlands,  
522 several limitations should be noted. (1) The model does not account for interannual changes in  
523 vegetation cover or species composition. Variations in plant functional types and leaf area index  
524 may influence soil moisture and HR, and incorporating these dynamics could improve long-term  
525 simulations. (2) Our analysis focused on the dominant tree species at study site; however, other  
526 plant species may also benefit from water redistributed by these trees, potentially influencing  
527 ecosystem water dynamics. (3) We did not include stem water refilling or nighttime transpiration  
528 reported by Howard et al. (2009) and Neumann et al. (2014), which may influence the  
529 magnitude of HR. (4) Finally, future studies should address these limitations and further  
530 investigate the role of HR in regulating ecosystem functions, such as carbon exchange and  
531 evapotranspiration.

#### 532 **5. Conclusions**

533 This study demonstrates the role of hydraulic redistribution (HR) in soil water dynamics in  
534 piñon-juniper woodlands. By integrating HR processes and observations into the Terrestrial  
535 Ecosystem Model (TECO) via data assimilation, we successfully constrained model soil  
536 hydraulics parameters and improved simulations of soil water content across multiple depths,  
537 particularly in shallow soil layers (0–30 cm) and during dry periods. Our model results indicate  
538 that HR rates vary in response to the duration of dry spells between rainfall events. Generally,  
539 HR rates tend to increase as soil becomes drier and decreases with increasing precipitation

540 magnitude and frequency. Across the wet to dry transition, HR rates exhibit a range of 0.10 to  
541 0.50 mm d<sup>-1</sup>. Consequently, HR increased soil moisture in topsoil layers by up to 60% during dry  
542 periods, with upward HR emerging as the dominant flux, especially in the top 30 cm. These  
543 findings underscore the potential influence of HR during dry periods and highlight its role in  
544 sustaining soil water availability for vegetation. Future research should explore how HR-  
545 mediated water redistribution affects ecosystem functions including carbon exchange, and  
546 evapotranspiration.

## 547 **6. Acknowledgments**

548 This research is supported by US Department of Energy's Office of Biological and  
549 Environmental Research, Environmental System Science (ESS) Program (DE-SC0023514 to  
550 WTP, MEL and YL) and the modeling effort used data collected with funding from the US  
551 National Science Foundation (IOS [1557176](#) to MEL, WTP, and Susan Schwinning). Additional  
552 support from US NSF grants (DEB 2242034, DEB 2406930, and DEB 2425290), the US  
553 Department of Energy's Terrestrial Ecosystem Sciences Grant DE-SC0023514, subcontract  
554 CW55561 from Oak Ridge National Laboratory to Cornell University, and the "NYS Connects:  
555 Climate Smart Farms & Forestry" project, funded by the USDA, the New York State Department  
556 of Environmental Conservation, and the New York State Department of Agriculture and  
557 Markets. This research is also part of AI-CLIMATE: "AI Institute for Climate-Land Interactions,  
558 Mitigation, Adaptation, Tradeoffs and Economy", funded by the USDA National Institute of  
559 Food and Agriculture (NIFA), the NSF National AI Research Institutes Competitive Award (No.  
560 2023-67021-39829) and Swiss National Foundation, Award#P500PN\_206603 for their financial  
561 support of this collaboration.

562 **7. Competing interests**

563 The authors declare no competing interests.

564 **8. Author contributions**

565 **AKC:** Conceptualization, Methodology, Data curation, Formal analysis, Writing - original draft.

566 **YZ:** Conceptualization, Writing - review & editing. **MC:** Writing - review & editing. **HD:**

567 Writing - review & editing, Data curation. **ML:** Conceptualization, Data curation, Supervision,

568 Writing - review & editing, Funding acquisition, Project administration. **WP:** Conceptualization,

569 Data curation, Supervision, Funding acquisition, Writing - review & editing. **YL:**

570 Conceptualization, Supervision, Project administration, Funding acquisition, Writing - review &

571 editing.

572 **9. Code availability**

573 The Terrestrial ECOsystem (TECO) model used in this paper is archived on Zenodo under

574 <https://doi.org/10.5281/zenodo.18201820>.

575 **10. Data availability**

576 The data supporting the findings of this study are available within the manuscript. Additional

577 data may be available upon request from the corresponding author, subject to compliance with

578 relevant data protection and privacy regulations.

579 **11. Supporting Information**

580 Supporting information accompanying this manuscript is available as a separate Word file. It

581 includes supplementary figures referenced in the main text.

582 **References**

583 Alfieri, J. G., Anderson, M. C., Kustas, W. P., and Cammalleri, C.: Effect of the revisit interval  
584 and temporal upscaling methods on the accuracy of remotely sensed evapotranspiration

585 estimates, *Hydrology and Earth System Sciences*, 21, 83-98, 10.5194/hess-21-83-2017,  
586 2017.

587 Amenu, G. G. and Kumar, P.: A model for hydraulic redistribution incorporating coupled soil-  
588 root moisture transport, *Hydrology and Earth System Sciences*, 12, 55-74, 10.5194/hess-  
589 12-55-2008, 2008.

590 Asadollahi, M., Nehemy, M. F., McDonnell, J. J., Rinaldo, A., and Benettin, P.: Toward a  
591 closure of catchment mass balance: Insight on the missing link from a vegetated  
592 lysimeter, *Water Resources Research*, 58, e2021WR030698, 2022.

593 Barron - Gafford, G. A., Knowles, J. F., Sanchez - Cañete, E. P., Minor, R. L., Lee, E., Sutter,  
594 L., Tran, N., Murphy, P., Hamerlynck, E. P., and Kumar, P.: Hydraulic redistribution  
595 buffers climate variability and regulates grass - tree interactions in a semiarid riparian  
596 savanna, *Ecohydrology*, 14, e2271, 2021.

597 Barron - Gafford, G. A., Sanchez - Cañete, E. P., Minor, R. L., Hendryx, S. M., Lee, E., Sutter,  
598 L. F., Tran, N., Parra, E., Colella, T., and Murphy, P. C.: Impacts of hydraulic  
599 redistribution on grass - tree competition vs facilitation in a semi - arid savanna, *New  
600 Phytologist*, 215, 1451-1461, 10.1111/nph.14693, 2017.

601 Beer, C., Reichstein, M., Tomelleri, E., Ciais, P., Jung, M., Carvalhais, N., Rödenbeck, C.,  
602 Arain, M. A., Baldocchi, D., and Bonan, G. B.: Terrestrial gross carbon dioxide uptake:  
603 global distribution and covariation with climate, *Science*, 329, 834-838, 2010.

604 Bleby, T. M., Mcelrone, A. J., and Jackson, R. B.: Water uptake and hydraulic redistribution  
605 across large woody root systems to 20 m depth, *Plant, cell & environment*, 33, 2132-  
606 2148, 2010.

607 Brooks, R. H.: *Hydraulic properties of porous media*, Colorado State University 1965.

608 Caldwell, M. M., Dawson, T. E., and Richards, J. H.: Hydraulic lift: consequences of water  
609 efflux from the roots of plants, *Oecologia*, 113, 151-161, 10.1007/s004420050363, 1998.

610 Campbell, G. S.: *Soil physics with BASIC: transport models for soil-plant systems*,  
611 Elsevier 1985.

612 Cattray, M., Miele, F., Wang, S., Frutschi, M., and Rinaldo, A.: Evaluating nitrate removal and  
613 travel times in a bare deciduous forest soil through a column tracer experiment, *Catena*,  
614 258, 109204, 2025.

615 Clapp, R. B. and Hornberger, G. M.: Empirical equations for some soil hydraulic properties,  
616 *Water resources research*, 14, 601-604, 1978.

617 Domec, J. C., King, J. S., Noormets, A., Treasure, E., Gavazzi, M. J., Sun, G., and McNulty, S.  
618 G.: Hydraulic redistribution of soil water by roots affects whole-stand evapotranspiration  
619 and net ecosystem carbon exchange, *New Phytol*, 187, 171-183, 10.1111/j.1469-  
620 8137.2010.03245.x, 2010.

621 Eastburn, J. F., Campbell, M. J., Dennison, P. E., Anderegg, W. R., Barrett, K. J., Fekety, P. A.,  
622 Flake, S. W., Huffman, D. W., Kannenberg, S. A., and Kerr, K. L.: Ecological and  
623 climatic transferability of airborne lidar-driven aboveground biomass models in Piñon-  
624 Juniper woodlands, *GIScience & Remote Sensing*, 61, 2363577, 2024.

625 Fabian, G. S., Sandra, J. B., William, A. H., Frederick, C. M., and Guillermo, G.: Hydraulic lift  
626 in a Neotropical savanna: Experimental manipulation and model simulations,  
627 *Agricultural and Forest Meteorology*, 150, 629-639, 10.1016/j.agrformet.2010.02.001,  
628 2010.

629 Fu, C. S., Wang, G. L., Goulden, M. L., Scott, R. L., Bible, K., and Cardon, Z. G.: Combined  
630 measurement and modeling of the hydrological impact of hydraulic redistribution using

631 CLM4.5 at eight AmeriFlux sites, *Hydrology and Earth System Sciences*, 20, 2001-2018,  
632 10.5194/hess-20-2001-2016, 2016.

633 Fu, C. S., Wang, G. L., Bible, K., Goulden, M. L., Saleska, S. R., Scott, R. L., and Cardon, Z. G.:  
634 Hydraulic redistribution affects modeled carbon cycling via soil microbial activity and  
635 suppressed fire, *Global Change Biology*, 24, 3472-3485, 10.1111/gcb.14164, 2018.

636 Grünzweig, J. M., De Boeck, H. J., Rey, A., Santos, M. J., Adam, O., Bahn, M., Belnap, J.,  
637 Deckmyn, G., Dekker, S. C., and Flores, O.: Dryland mechanisms could widely control  
638 ecosystem functioning in a drier and warmer world, *Nature ecology & evolution*, 6, 1064-  
639 1076, 2022.

640 Hafner, B. D., Hesse, B. D., Bauerle, T. L., and Grams, T. E.: Water potential gradient, root  
641 conduit size and root xylem hydraulic conductivity determine the extent of hydraulic  
642 redistribution in temperate trees, *Functional Ecology*, 34, 561-574, 2020.

643 Hao, X. M., Chen, Y. N., Guo, B., and Ma, J. X.: Hydraulic redistribution of soil water in  
644 *Populus euphratica* Oliv. in a central Asian desert riparian forest, *Ecohydrology*, 6, 974-  
645 983, 10.1002/eco.1338, 2013a.

646 Hao, X. M., Li, W. H., Guo, B., and Ma, J. X.: Simulation of the effect of root distribution on  
647 hydraulic redistribution in a desert riparian forest, *Ecological research*, 28, 653-662,  
648 2013b.

649 Hastings, W. K.: Monte Carlo sampling methods using Markov chains and their applications,  
650 1970.

651 Hillel, D.: Introduction to environmental soil physics, Elsevier2003.

652 Hou, E., Litvak, M. E., Rudgers, J. A., Jiang, L., Collins, S. L., Pockman, W. T., Hui, D., Niu, S.,  
653 and Luo, Y.: Divergent responses of primary production to increasing precipitation  
654 variability in global drylands, *Glob Chang Biol*, 27, 5225-5237, 10.1111/gcb.15801,  
655 2021.

656 Howard, A. R., Van Iersel, M. W., Richards, J. H., and Donovan, L. A.: Night - time  
657 transpiration can decrease hydraulic redistribution, *Plant, Cell & Environment*, 32, 1060-  
658 1070, 2009.

659 Hultine, K. R., Cable, W. L., Burgess, S. S. O., and Williams, D. G.: Hydraulic redistribution by  
660 deep roots of a Chihuahuan Desert phreatophyte, *Tree Physiology*, 23, 353-360, DOI  
661 10.1093/treephys/23.5.353, 2003.

662 Jiang, J., Huang, Y., Ma, S., Stacy, M., Shi, Z., Ricciuto, D. M., Hanson, P. J., and Luo, Y.:  
663 Forecasting responses of a northern peatland carbon cycle to elevated CO<sub>2</sub> and a gradient  
664 of experimental warming, *Journal of Geophysical Research: Biogeosciences*, 123, 1057-  
665 1071, 10.1002/2017jg004040, 2018.

666 Katul, G. G. and Siqueira, M. B.: Biotic and abiotic factors act in coordination to amplify  
667 hydraulic redistribution and lift, *The New Phytologist*, 187, 3-6, 2010.

668 Kohler, M. A. and Linsley, R. K.: Predicting the runoff from storm rainfall, US Department of  
669 Commerce, Weather Bureau1951.

670 Lee, E., Kumar, P., Barron-Gafford, G. A., Hendryx, S. M., Sanchez-Cañete, E. P., Minor, R. L.,  
671 Colella, T., and Scott, R. L.: Impact of hydraulic redistribution on multispecies vegetation  
672 water use in a semiarid savanna ecosystem: An experimental and modeling synthesis,  
673 *Water Resources Research*, 54, 4009-4027, 10.1029/2017wr021006, 2018.

674 Li, X., Wei, Y., and Li, F.: Optimality of antecedent precipitation index and its application,  
675 *Journal of Hydrology*, 595, 126027, 2021.

676 Luo, Y. and Reynolds, J. F.: Validity of extrapolating field CO<sub>2</sub> experiments to predict carbon  
677 sequestration in natural ecosystems, *Ecology*, 80, 1568-1583, 10.1890/0012-  
678 9658(1999)080[1568:Voefce]2.0.Co;2, 1999.

679 Luo, Y. and Schuur, E. A. G.: Model parameterization to represent processes at unresolved  
680 scales and changing properties of evolving systems, *Glob Chang Biol*, 26, 1109-1117,  
681 10.1111/gcb.14939, 2020.

682 Marshall, L., Nott, D., and Sharma, A.: A comparative study of Markov chain Monte Carlo  
683 methods for conceptual rainfall - runoff modeling, *Water Resources Research*, 40, 2004.

684 Meinzer, F. C., Brooks, J. R., Bucci, S., Goldstein, G., Scholz, F. G., and Warren, J. M.:  
685 Converging patterns of uptake and hydraulic redistribution of soil water in contrasting  
686 woody vegetation types, *Tree Physiology*, 24, 919-928, 10.1093/treephys/24.8.919, 2004.

687 Metropolis, N., Rosenbluth, A. W., Rosenbluth, M. N., Teller, A. H., and Teller, E.: Equation of  
688 state calculations by fast computing machines, *The journal of chemical physics*, 21,  
689 1087-1092, 1953.

690 Miele, F., Benettin, P., Wang, S., Retti, I., Asadollahi, M., Frutschi, M., Mohanty, B., Bernier -  
691 Latmani, R., and Rinaldo, A.: Spatially explicit linkages between redox potential cycles  
692 and soil moisture fluctuations, *Water Resources Research*, 59, e2022WR032328, 2023.

693 Mosegaard, K. and Sambridge, M.: Monte Carlo analysis of inverse problems, *Inverse problems*,  
694 18, R29, 2002.

695 Nadezhdina, N., Ferreira, M. I., Conceição, N., Pacheco, C. A., Häusler, M., and David, T. S.:  
696 Water uptake and hydraulic redistribution under a seasonal climate: long - term study in  
697 a rainfed olive orchard, *Ecohydrology*, 8, 387-397, 2015.

698 Nadezhdina, N., David, T. S., David, J. S., Ferreira, M. I., Dohnal, M., Tesař, M., Gartner, K.,  
699 Leitgeb, E., Nadezhdin, V., and Cermak, J.: Trees never rest: the multiple facets of  
700 hydraulic redistribution, *Ecohydrology*, 3, 431-444, 2010.

701 Neumann, R. B. and Cardon, Z. G.: The magnitude of hydraulic redistribution by plant roots: a  
702 review and synthesis of empirical and modeling studies, *New Phytol*, 194, 337-352,  
703 10.1111/j.1469-8137.2012.04088.x, 2012.

704 Neumann, R. B., Cardon, Z. G., TESHARA - LEVYE, J., Rockwell, F. E., Zwieniecki, M. A.,  
705 and Holbrook, N. M.: Modelled hydraulic redistribution by sunflower (*H. elianthus*  
706 *annuus* L.) matches observed data only after including night - time transpiration, *Plant*,  
707 *Cell & Environment*, 37, 899-910, 2014.

708 Nicola, M. and Ram, O.: Rhizosphere water content drives hydraulic redistribution: Implications  
709 of pore-scale heterogeneity to modeling diurnal transpiration in water-limited  
710 ecosystems, *Agricultural and Forest Meteorology*, 312,  
711 10.1016/j.agrformet.2021.108720, 2022.

712 Novick, K. A., Ficklin, D. L., Baldocchi, D., Davis, K. J., Ghezzehei, T. A., Konings, A. G.,  
713 MacBean, N., Raoult, N., Scott, R. L., and Shi, Y.: Confronting the water potential  
714 information gap, *Nature Geosci*, 15, 158-164, 2022.

715 Práválie, R.: Drylands extent and environmental issues. A global approach, *Earth-Science*  
716 *Reviews*, 161, 259-278, 2016.

717 Prieto, I., Armas, C., and Pugnaire, F. I.: Water release through plant roots: new insights into its  
718 consequences at the plant and ecosystem level, *New Phytol*, 193, 830-841,  
719 10.1111/j.1469-8137.2011.04039.x, 2012.

720 Priyadarshini, K. V. R., Prins, H. H. T., de Bie, S., Heitkönig, I. M. A., Woodborne, S., Gort, G.,  
721 Kirkman, K., Ludwig, F., Dawson, T. E., and de Kroon, H.: Seasonality of hydraulic

722 redistribution by trees to grasses and changes in their water - source use that change  
723 tree - grass interactions, *Ecohydrology*, 9, 218-228, 10.1002/eco.1624, 2016.

724 Quijano, J. C. and Kumar, P.: Numerical simulations of hydraulic redistribution across climates:  
725 The role of the root hydraulic conductivities, *Water Resources Research*, 51, 8529-8550,  
726 10.1002/2014wr016509, 2015.

727 Rawls, W. J., Brakensiek, D. L., and Saxton, K.: Estimation of soil water properties,  
728 *Transactions of the ASAE*, 25, 1316-1320, 1982.

729 Romme, W. H., Allen, C. D., Bailey, J. D., Baker, W. L., Bestelmeyer, B. T., Brown, P. M.,  
730 Eisenhart, K. S., Floyd, M. L., Huffman, D. W., and Jacobs, B. F.: Historical and modern  
731 disturbance regimes, stand structures, and landscape dynamics in pinon–juniper  
732 vegetation of the western United States, *Rangeland Ecology & Management*, 62, 203-  
733 222, 2009.

734 Ryel, R., Caldwell, M., Yoder, C., Or, D., and Leffler, A.: Hydraulic redistribution in a stand of  
735 *Artemisia tridentata*: evaluation of benefits to transpiration assessed with a simulation  
736 model, *Oecologia*, 130, 173-184, 10.1007/s004420100794, 2002.

737 Saito, T., Fujimaki, H., Yasuda, H., and Inoue, M.: Empirical temperature calibration of  
738 capacitance probes to measure soil water, *Soil Science Society of America Journal*, 73,  
739 1931-1937, 2009.

740 Sardans, J. and Peñuelas, J.: Hydraulic redistribution by plants and nutrient stoichiometry: Shifts  
741 under global change, *Ecohydrology*, 7, 1-20, 2014.

742 Schwinning, S., Litvak, M. E., Pockman, W. T., Pangle, R. E., Fox, A. M., Huang, C. W., and  
743 McIntire, C. D.: A 3-dimensional model of *Pinus edulis* and *Juniperus monosperma* root  
744 distributions in New Mexico: implications for soil water dynamics, *Plant Soil*, 450, 337-  
745 355, 10.1007/s11104-020-04446-y, 2020.

746 Scott, R. L., Cable, W. L., and Hultine, K. R.: The ecohydrologic significance of hydraulic  
747 redistribution in a semiarid savanna, *Water Resources Research*, 44,  
748 10.1029/2007wr006149, 2008.

749 Seneviratne, S. I., Corti, T., Davin, E. L., Hirschi, M., Jaeger, E. B., Lehner, I., Orlowsky, B.,  
750 and Teuling, A. J.: Investigating soil moisture–climate interactions in a changing climate:  
751 A review, *Earth-Science Reviews*, 99, 125-161, 2010.

752 Tang, J., Riley, W. J., and Niu, J.: Incorporating root hydraulic redistribution in CLM 4.5:  
753 Effects on predicted site and global evapotranspiration, soil moisture, and water storage,  
754 *Journal of Advances in Modeling Earth Systems*, 7, 1828-1848, 2015.

755 Ukkola, A. M., De Kauwe, M. G., Roderick, M. L., Burrell, A., Lehmann, P., and Pitman, A. J.:  
756 Annual precipitation explains variability in dryland vegetation greenness globally but not  
757 locally, *Global Change Biology*, 27, 4367-4380, 2021.

758 Wei, L., Qiu, Z., Zhou, G., Zuecco, G., Liu, Y., and Wen, Y.: Soil water hydraulic redistribution  
759 in a subtropical monsoon evergreen forest, *Science of The Total Environment*, 835,  
760 155437, 10.1016/j.scitotenv.2022.155437, 2022.

761 Weng, E. and Luo, Y.: Soil hydrological properties regulate grassland ecosystem responses to  
762 multifactor global change: A modeling analysis, *Journal of Geophysical Research:  
763 Biogeosciences*, 113, 10.1029/2007jg000539, 2008.

764 Williams, M., Rastetter, E., Fernandes, D., Goulden, M., Wofsy, S., Shaver, G., Melillo, J.,  
765 Munger, J., Fan, S. M., and Nadelhoffer, K.: Modelling the soil - plant - atmosphere  
766 continuum in a *Quercus* - *Acer* stand at Harvard Forest: The regulation of stomatal

767 conductance by light, nitrogen and soil/plant hydraulic properties, *Plant, Cell &*  
768 *Environment*, 19, 911-927, 1996.

769 Willmott, C. J. and Matsuura, K.: Advantages of the mean absolute error (MAE) over the root  
770 mean square error (RMSE) in assessing average model performance, *Climate research*,  
771 30, 79-82, 2005.

772 Wu, H., Fu, C., Wu, H., and Zhang, L.: Influence of the dry event induced hydraulic  
773 redistribution on water and carbon cycles at five AsiaFlux forest sites: A site study  
774 combining measurements and modeling, *Journal of Hydrology*, 587, 124979,  
775 10.1016/j.jhydrol.2020.124979, 2020.

776 Xu, T., White, L., Hui, D., and Luo, Y.: Probabilistic inversion of a terrestrial ecosystem model:  
777 Analysis of uncertainty in parameter estimation and model prediction, *Global*  
778 *Biogeochemical Cycles*, 20, 10.1029/2005gb002468, 2006.

779 Yan, B. and Dickinson, R. E.: Modeling hydraulic redistribution and ecosystem response to  
780 droughts over the Amazon basin using Community Land Model 4.0 (CLM4), *Journal of*  
781 *Geophysical Research: Biogeosciences*, 119, 2130-2143, 10.1002/2014jg002694, 2014.

782 Yang, G., Huang, L., and Shi, Y.: Magnitude and determinants of plant root hydraulic  
783 redistribution: A global synthesis analysis, *Frontiers in Plant Science*, 13, 918585, 2022.

784 Yu, K. L. and D'Odorico, P.: Climate, vegetation, and soil controls on hydraulic redistribution in  
785 shallow tree roots, *Advances in Water Resources*, 66, 70-80,  
786 10.1016/j.advwatres.2014.02.003, 2014.

787 Yu, T., Feng, Q., Si, J., Xi, H., Li, Z., and Chen, A.: Hydraulic redistribution of soil water by  
788 roots of two desert riparian phreatophytes in northwest China's extremely arid region,  
789 *Plant Soil*, 372, 297-308, 10.1007/s11104-013-1727-8, 2013.

790 Zhang, D., Madsen, H., Ridler, M. E., Kidmose, J., Jensen, K. H., and Refsgaard, J. C.:  
791 Multivariate hydrological data assimilation of soil moisture and groundwater head,  
792 *Hydrology and Earth System Sciences*, 20, 4341-4357, 2016.

793 Zheng, Z. and Wang, G.: Modeling the dynamic root water uptake and its hydrological impact at  
794 the Reserva Jaru site in Amazonia, *Journal of Geophysical Research: Biogeosciences*,  
795 112, 2007.

796 Zhu, S., Chen, H., Zhang, X., Wei, N., Shangguan, W., Yuan, H., Zhang, S., Wang, L., Zhou, L.,  
797 and Dai, Y.: Incorporating root hydraulic redistribution and compensatory water uptake  
798 in the Common Land Model: Effects on site level and global land modeling, *Journal of*  
799 *Geophysical Research: Atmospheres*, 122, 7308-7322, 2017.

800